Article

TRANSPARENT PROCESS

THE EMBO JOURNAL

Structural basis for processivity and antiviral drug toxicity in human mitochondrial DNA replicase

Michal R Szymanski[1,2], Vladmir B Kuznetsov[1,2,†], Christie Shumate[1,2,†], Qingchao Meng[1], Young-Sam Lee[1], Gayatri Patel[3], Smita Patel[3] & Y Whitney Yin[1,2,*]

Abstract

The human DNA polymerase gamma (Pol γ) is responsible for DNA replication in mitochondria. Pol γ is particularly susceptible to inhibition by dideoxynucleoside-based inhibitors designed to fight viral infection. Here, we report crystal structures of the replicating Pol γ–DNA complex bound to either substrate or zalcitabine, an inhibitor used for HIV reverse transcriptase. The structures reveal that zalcitabine binds to the Pol γ active site almost identically to the substrate dCTP, providing a structural basis for Pol γ-mediated drug toxicity. When compared to the apo form, Pol γ undergoes intra- and inter-subunit conformational changes upon formation of the ternary complex with primer/template DNA and substrate. We also find that the accessory subunit Pol γB, which lacks intrinsic enzymatic activity and does not contact the primer/template DNA directly, serves as an allosteric regulator of holoenzyme activities. The structures presented here suggest a mechanism for processivity of the holoenzyme and provide a model for understanding the deleterious effects of Pol γ mutations in human disease. Crystal structures of the mitochondrial DNA polymerase, Pol γ, in complex with substrate or antiviral inhibitor zalcitabine provide a basis for understanding Pol γ-mediated drug toxicity.

Keywords DNA replication; drug toxicity; human DNA polymerase gamma; mitochondrial toxicity; nucleoside reverse transcriptase inhibitors
Subject Categories DNA Replication, Repair & Recombination; Structural Biology
DOI 10.15252/embj.201591520 | Received 13 March 2015 | Revised 24 April 2015 | Accepted 18 May 2015 | Published online 8 June 2015
The EMBO Journal (2015) 34: 1959–1970

Introduction

A human mitochondrion DNA (mtDNA) codes for a subset of components of the oxidative phosphorylation electron transfer chain for ATP synthesis. The integrity of mtDNA is critically important for energy supplies, the cell cycle, and programmed cell death. Mutations in both human mtDNA and mitochondrial DNA polymerase (Pol γ) have been associated with multisystem clinical disorders (Stumpf & Copeland, 2013).

Unlike nuclear DNA polymerases that have specialized functions in either replication or repair, Pol γ is responsible for both mtDNA replication and repair. Human Pol γ holoenzyme consists of a catalytic subunit Pol γA and a dimeric accessory subunit Pol γB. Pol γA possesses all active sites for holoenzyme activities, including polymerization (*pol*) for DNA synthesis, 3′–5′ exonuclease (*exo*) for proofreading, and 5′ deoxyribophosphate (5′dRP) lyase for base excision repair. Pol γB has no intrinsic enzymatic activity, but regulates all Pol γA activities in the holoenzyme (Longley *et al*, 1998; Johnson *et al*, 2000; Gellon *et al*, 2008).

Structurally, Pol γ belongs to the DNA Pol I family. Polymerases in this family dissociate from DNA frequently and are therefore unsuitable for efficient highly processive DNA replication. Indeed, Pol γA alone displays low processivity (Graves *et al*, 1998; Lim *et al*, 1999). However, in contrast to most Pol I family members, Pol γA has a spacer domain that enables it to associate with Pol γB; the resulting holoenzyme exhibits drastically increased processivity (Graves *et al*, 1998; Lim *et al*, 1999). Pol γB enhances the holoenzyme's processivity by both increasing the affinity of the holoenzyme for DNA and accelerating the DNA synthesis reaction rate (Johnson *et al*, 2000; Lee *et al*, 2010b). Pol γB also increases 5′dRP lyase and reduces exonucleolytic activities (Pinz & Bogenhagen, 2006). A crystal structure of apo Pol γ shows that the *pol* and *exo* active sites are 35 Å apart, and it is unclear how Pol γB can regulate multiple activities. Pol γA contacts dimeric Pol γB asymmetrically: It interacts extensively with the proximal Pol γB monomer, but only minimally with the distal monomer (Lee *et al*, 2009). Nevertheless, subunit interactions at the distal monomer region are important for proper functioning of the holoenzyme, as evidenced by the observation that Pol γA mutants (R232G or R232H) that reside at Pol γA–distal Pol γB subunit interface show significantly reduced DNA synthesis activity and elevated exonucleolytic activity. Patients carrying Pol γA mutations R232G/H display muscular and neurological disorders (Ferrari *et al*, 2005; Kollberg *et al*, 2006; Lee *et al*, 2010a; Rouzier *et al*, 2014). The apo structure provides little insight as to why these mutations give rise to the resulting phenotype.

1 Department of Pharmacology and Toxicology, University of Texas Medical Branch, Galveston, TX, USA
2 Sealy Center for Structural Biology, University of Texas Medical Branch, Galveston, TX, USA
3 Biochemistry and Molecular Biology, Rutgers-Robert Wood Johnson Medical School, Piscataway, NJ, USA
*Corresponding author. Tel: +1 409 772 9631; E-mail: ywyin@utmb.edu
†These authors contributed equally to this work

The error frequency of Pol γ is 10^{-5} during DNA replication, comparable to other high-fidelity DNA polymerases (Longley *et al*, 2001; Lee & Johnson, 2006). However, Pol γ displays lower discrimination than its nuclear counterparts against nucleoside analog HIV reverse transcriptase inhibitors (NRTIs), particularly dideoxynucleoside triphosphates (Johnson *et al*, 2001; Lee *et al*, 2003). Thus, the NRTIs that inhibit Pol γ result in moderate to life-threatening mitochondrial toxicity (McKenzie *et al*, 1995; Koczor & Lewis, 2010).

To understand antiviral drug toxicity and Pol γ mutations in human diseases, we determined crystal structures of Pol γ holoenzyme replication complexes, captured with either a substrate or an antiviral agent, zalcitabine. These structures are the first intact multi-subunit DNA replicase captured during DNA synthesis. The structures illustrate how the two subunits coordinate functions in the holoenzyme to achieve high processivity and to regulate *pol*/*exo* activities. The structures show that Pol γ binds zalcitabine and a substrate almost identically, providing a molecular basis for Pol γ's susceptibility to inhibition by dideoxynucleotides. The structures provide new insight in understanding diseases associated with Pol γ mutations that were inexplicable by the apo structure.

Results and Discussion

Overall structure of replicating holoenzyme

Crystals of human Pol γ replicating complexes (~250 kDa) were formed in the presence of the catalytic subunit Pol γA, the accessory subunit Pol γB, a 24/28-mer primer/template duplex DNA, $CaCl_2$, and a substrate (dCTP), or a NRTI (the triphosphate form of zalcitabine, ddCTP) (Fig 1). Pol γB adopts a pyramidal configuration resembling class II aminoacyl tRNA synthetases with domains corresponding to the base, middle, and apex of the pyramid. Pol γA has three domains: a polymerase (*pol)* domain that has the canonical "right-hand" DNA polymerase fold with subdomains called the thumb, fingers, and palm; an exonuclease (*exo*) domain; and a spacer domain that lies between *pol* and *exo*. The Pol γA spacer domain contains two subdomains: a globular intrinsic processivity (IP) subdomain and an extended accessory-interacting determinant (AID) subdomain that forms a major binding site for Pol γB at the proximal monomer (Supplementary Fig S1). The primer/template DNA is located in a deep positively charged cleft on Pol γA. Relative to the apo holoenzyme, where Pol γA has almost no interaction with the distal Pol γB monomer, the replication complex has significantly enhanced interaction between the distal Pol γB monomer and Pol γA at the R^{232} region, resulting from DNA-binding-induced conformational changes. The newly formed subunit interface plays an important role in enabling Pol γB to allosterically regulate polymerase and exonuclease activities in the holoenzyme. The structures illustrate the division of functions in a multi-subunit DNA polymerase.

Substrate, inhibitor, and DNA-binding sites

In the replication complex, the substrate dCTP is coordinated by the catalytic residues D^{890} and D^{1135} and two metal ions (M^{2+}) in the *pol* active site bounded by the palm and fingers subdomains (Fig 2; Supplementary Fig S2). Although as many as four metal ions are seen in various DNA polymerases, a minimum of two metal ions are critical for the phosphotransfer reaction. One divalent metal ion participates in nucleophilic reaction by reducing the pKa of the attacking group, 3′OH of the primer. The other metal ion stabilizes the leaving group PPi after catalysis (Steitz & Steitz, 1993). As the primer terminus is a nonreactive dideoxynucleotide, the structure represents a pre-chemistry substrate complex (Steitz, 1999). The triphosphate moiety of dCTP is stabilized by R^{943} and K^{947} of the O-helix (residues 943–955) in the fingers subdomain (Fig 3). The template DNA bends ~90° at the single-/double-strand junction; the bent conformation is enforced by Y^{955} and a short connecting loop (^{957}AG^{958}) (Fig 2). Compared to apo Pol γ, the O-helix pivots around its center so that R^{943} and K^{947} close the active site concurrent with Y^{955} rotation to facilitate productive dNTP binding (Fig 4B). This extreme template bending and Y^{955} rotation are important to maintain template register, and to reduce slippage and backtracking during replication (Graziewicz *et al*, 2004; Estep & Johnson, 2011). The open–closed conformational change occurs at each nucleotide addition, as shown in many high-fidelity DNA polymerases (Doublié & Ellenberger, 1998; Steitz & Yin, 2004).

The DNA duplex is bound exclusively to Pol γA in a deep crevice formed by the spacer and *pol* domains, adopting the A-form in the active site, and transforming to B-form around base pair −4. All subdomains of Pol γA *pol* domain participate in interacting with the primer/template DNA (Fig 3). The thumb binds the minor groove of the duplex at the −5 to −7 positions, and a cluster of positively charged residues, R^{802}, K^{806}, and R^{807}, forms electrostatic interactions with the DNA backbone (Figs 3 and 4A; Supplementary Fig S3). These interactions made us predict that the thumb forms firm grip on the DNA duplex such that movements of the thumb are coupled to movements of the primer terminus.

Additional DNA interactions are formed with the spacer domain: The IP subdomain binds the primer strand at positions −3 to −5. Together with *pol*, the IP subdomain encircles the primer/template, reducing enzyme dissociation from the DNA. The flexible AID subdomain contains a lysine-rich K-tract that interacts with the negatively charged phosphodiester backbone (Fig 4A). Binding to Pol γB stabilizes the flexible AID subdomain and increases the holoenzyme DNA-binding area to 20 bp from that of 10 bp with Pol γA alone. The increased interaction provides a structural basis for Pol γB increasing DNA affinity in the holoenzyme.

The replication complex containing ddCTP shows that the inhibitor is bound nearly identically as dCTP (Fig 2; Supplementary Fig S2), providing a structural basis for the high toxicity for ddN-based antiviral inhibitors. In both structures, Y^{951} stacks with the incoming nucleotide, with its –OH group that is 3.5 Å from O3′ and C2′ of the deoxyribose moiety. The hydroxyl group of Y^{951} is the main source of drug toxicity, because the Pol γA Y951F mutant exhibits significantly reduced sensitivity to ddN (Lim *et al*, 2003; Graziewicz *et al*, 2004). E895 is situated in the *pol* site, and its ε-oxygen is 3.4 and 4.3 Å from the C2′ and O3′ of the ribose moiety of dCTP, confirming its contributions to rNTP and minor ddNTP discrimination (Supplementary Fig S4). In Pol I family members, this residue, conserved as either a Phe or Tyr, is important for substrate sugar moiety specificity (Tabor & Richardson, 1995; Astatke *et al*, 1998; Feng *et al*, 2004). Although both Phe and Tyr are able to discriminate against the ribonucleotides that are structurally larger than dNTP, only Phe exhibits selectivity against smaller ddNTP (Tabor & Richardson, 1995; Astatke *et al*, 1998; Wang *et al*, 2012). Pol γA Y951F substitution is likely to

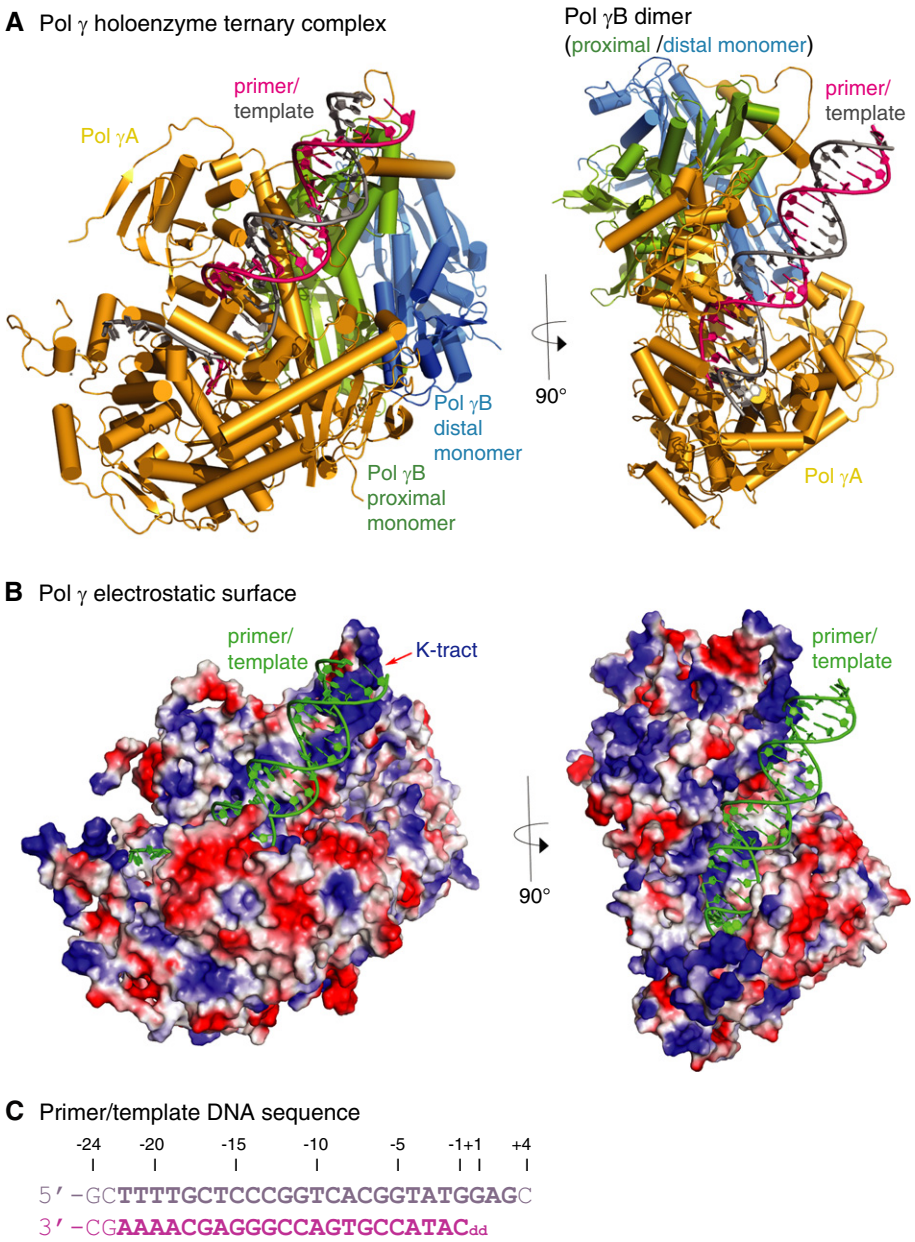

Figure 1. Structure of Pol γ replication complex.

A Pol γ holoenzyme ternary complex contains Pol γA, a dimeric Pol γB with the proximal (green) and the distal monomers (blue), a primer/template (pink/gray) DNA duplex, and an incoming nucleotide.

B Pol γ (shown in electrostatic surface) interaction with primer/template DNA (green).

C Primer/template DNA sequence. The structurally visible region of the primer/template is bolded in the sequences. For convenience, bases are number such that the incoming nucleotide is +1, and the upstream residues are −1, −2, . . ., n, and the downstream residues +2, +4.

cause a slight misalignment of the O-helix, resulting in exclusion of ddNTP in a fashion similar to that shown in bacillus DNAP ternary complexes (Wang *et al*, 2012).

DNA induced intra- and inter-subunit structural changes

Upon binding to DNA, the holoenzyme undergoes conformational changes that reveal the mechanism for holoenzyme processivity and *pol* and *exo* activity regulation. In the apo enzyme, the subunit interface is formed between proximal Pol γB monomer and Pol γA L-helix in the AID and the thumb subdomains; only a single salt bridge exists between R^{232} and E^{394} of the distal Pol γB monomer (Fig 5A and B). Formation of a productive replication complex results in conformational changes at the subunit interface: Pol γB rotates by 22° toward *pol* of Pol γA. However, the rotation does not alter the interface of Pol γA–Pol γB proximal monomer because the thumb and the

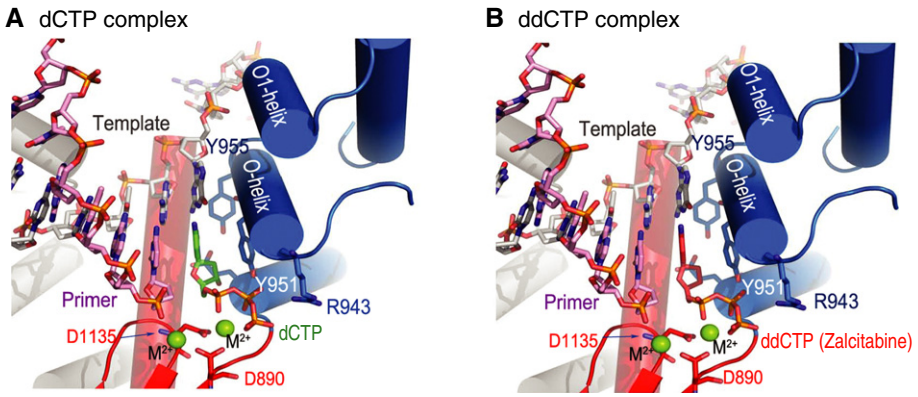

Figure 2. The *pol* active site of Pol γ ternary complex.

A The *pol* active site of a Pol γ ternary complex with a substrate dCTP.

B The *pol* active site of a Pol γ ternary complex with inhibitor ddCTP (zalcitabine).

L-helix of Pol γA rotate together with Pol γB as a single rigid body, despite being on separate polypeptide chains. These conformational changes bring the Pol γB distal monomer 16 Å closer to Pol γA in the R232 region (Fig 5C). Consequently, a more substantial subunit interaction is formed between Pol γA and distal Pol γB monomer; the contact surface area increases from 226 $Å^2$ in the apo enzyme to 1,610 $Å^2$ in the ternary replication complex. Using the conversion factor of 25 cal per $Å^2$ contact surface area (Richards, 1977), the conformational changes enhance the interaction of Pol γA with the distal Pol γB monomer by 34 kcal. Importantly, Pol γA R^{232} is situated in a pocket of the distal Pol γB, forming H-bonds with H^{467} and S^{469}, and Pol γA W^{235} forms hydrophobic interactions with Pol γB V^{338} (Fig 5C). The replication complex adopts a more compact structure than apo Pol γ in good agreement with solution measurement performed by small-angle X-ray scattering (He *et al*, 2013). While Pol γA displays several intra-subunit-independent structural changes in the fingers, thumb and L-helix, and the IP subdomains, Pol γB shows no internal structural changes and moves as a rigid body. The locations of Pol γB and the Pol γA thumb in the replication complex orient the primer terminus in *pol* and away from *exo*, tilting the *pol*/*exo* activity balance toward replication. The structure provides an explanation for the deleterious effects on mtDNA synthesis in patients carrying Pol γA R^{232} substitutions and highlights the importance of an intact Pol γA–distal Pol γB monomer interface for mitochondrial DNA replication.

The two subdomains in the spacer undergo different modes of structural changes upon binding to DNA (Figs 4A and 5A). The IP globular subdomain clamps down on the DNA duplex toward the 3′-end of the primer, enlarging the Pol γA DNA-binding site, whereas the AID subdomain undergoes more complex changes. The

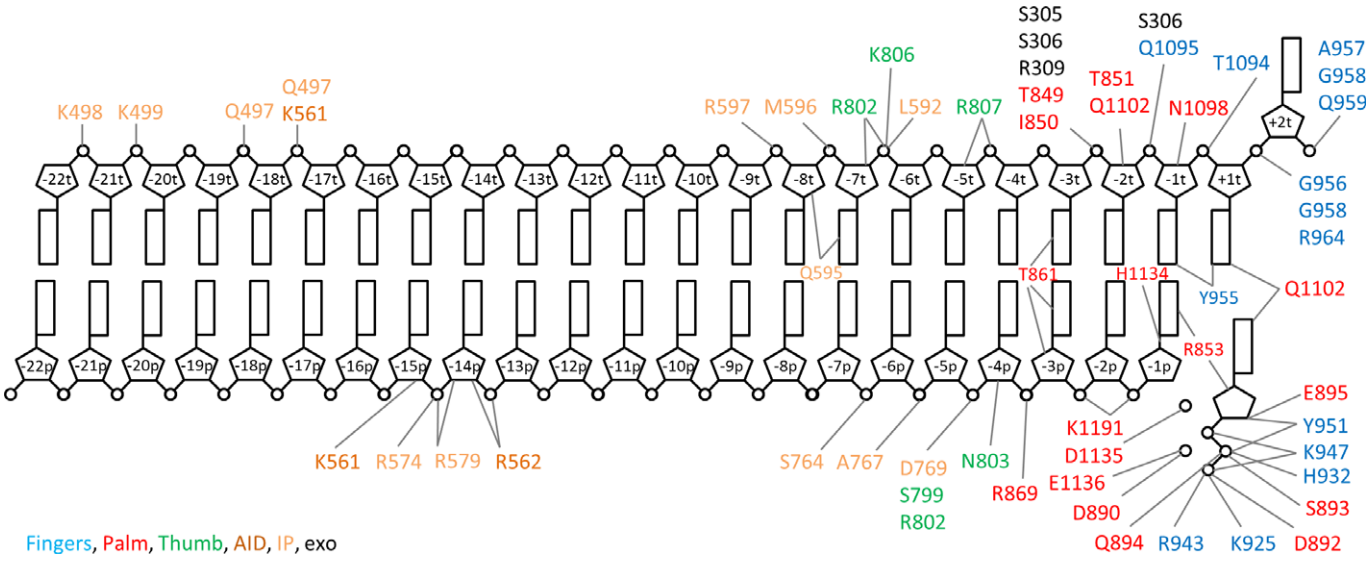

Figure 3. Schematic representation of Pol γ–DNA interactions.

Residues are color-coded with *exo* domain residues in black, spacer domain: IP subdomain in yellow, AID subdomain in orange, *pol* domain containing subdomains palm (red), fingers (blue) and thumb (green).

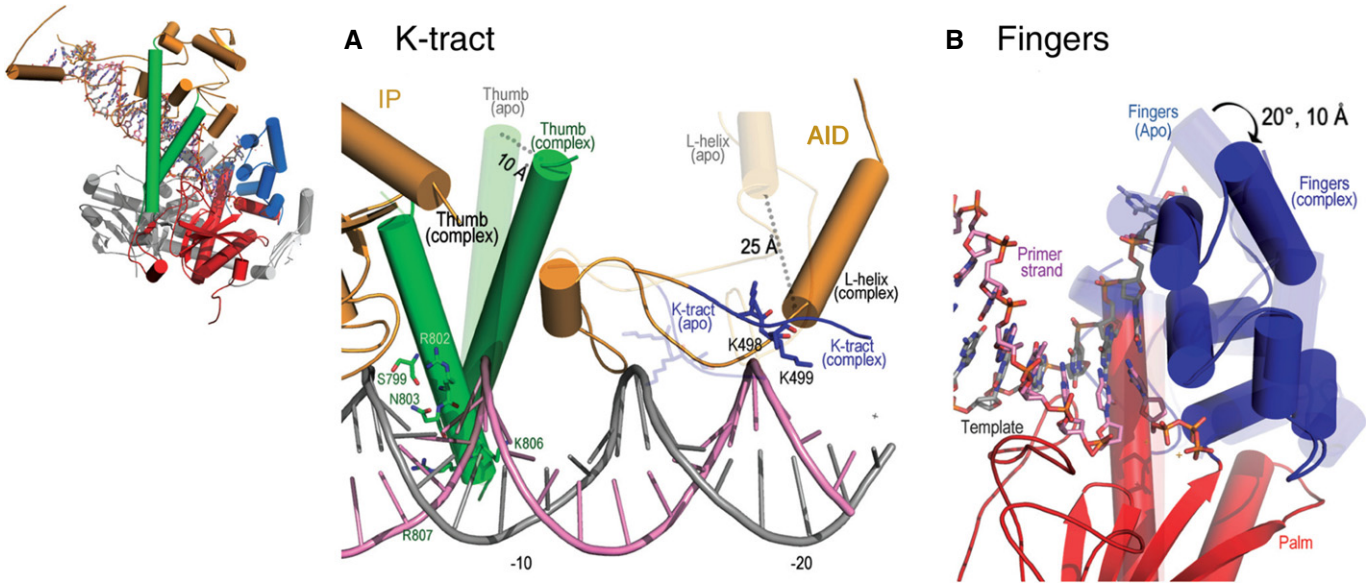

Figure 4. Conformational changes induced by DNA binding.

A The K-tract region moves 25 Å from its position in the apo enzyme (light colors) to the replication complex (solid colors).
B The fingers move 20° (10 Å) from the open conformation in apo (light blue) to the closed form in the complex (dark blue).

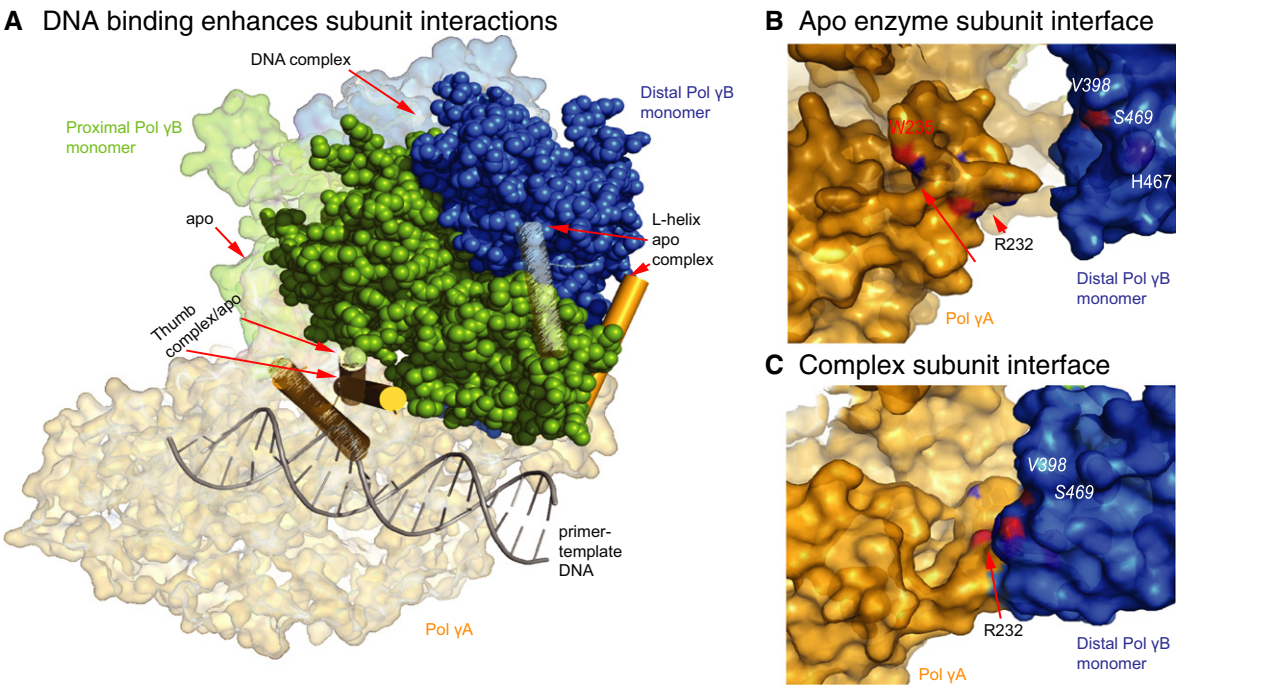

Figure 5. The inter-subunit conformational changes from apo to ternary complex.

A Pol γB and its binding elements in Pol γA, the thumb and the L-helix rotate 22° as a rigid body.
B The distal Pol γB monomer moves 16 Å from its position in apo to complex position as shown in (C).
C The complex.

lysine-rich K-tract binds DNA duplex in the minor groove at base pairs −20 to −22 (Figs 3 and 4A), and additional interactions are seen between AID and the distal Pol γB monomer (Fig 4A). These structural changes are consistent with solution studies where binding to DNA strengthens the affinity of Pol γA for Pol γB (Lee *et al*, 2010b). A pre-steady state kinetic study reported that Pol γ exhibits reduced

synthesis rate on a 18-nt primer, which is sevenfold slower than that on a 24-nt primer (3.2 nt s^{-1} versus 22 nt s^{-1}) (Murakami *et al*, 2003), in good agreement with our structural results.

To confirm our structural results, we substituted each lysine in the K-tract to cysteine and analyzed the pre-steady state kinetics of multiple nucleotide addition by Pol γ variants using primer/template substrate in the presence of all dNTPs. The rationale for the substitutions was to examine the effect of positive-charge changes on DNA synthesis activity. 25-nt primer was used as Pol γ synthesis rate on primers 25 nt or longer provided maximum reaction rate, as analyses using longer primers (up to 37 nt) showed that Pol γ replication proceeds at comparable rate as on the 25-nt primer. Thus, 25-nt primer is the minimal length primer that enables the maximum reaction rate for Pol γ. Pol γA elongates the primer at an average rate of 14 nt s^{-1}, whereas Pol γ holoenzyme is more efficient at an average rate of 43 nt s^{-1}. This processive elongation rate of the holoenzyme is very similar to the rate of single-nucleotide addition reported in the literature (Estep & Johnson, 2011). The K-tract substitutions (K498C, K499C, and K501C) have a significant effect on the activity of both Pol γA and holoenzyme (Fig 6). In the absence of Pol γB, the mutants add the first nucleotide rapidly, but subsequent nucleotides are added at two- to fivefold slower rates relative to wild-type. Therefore, in these mutants, there is visible accumulation of the one-nucleotide elongation product even in the presence of all dNTPs.

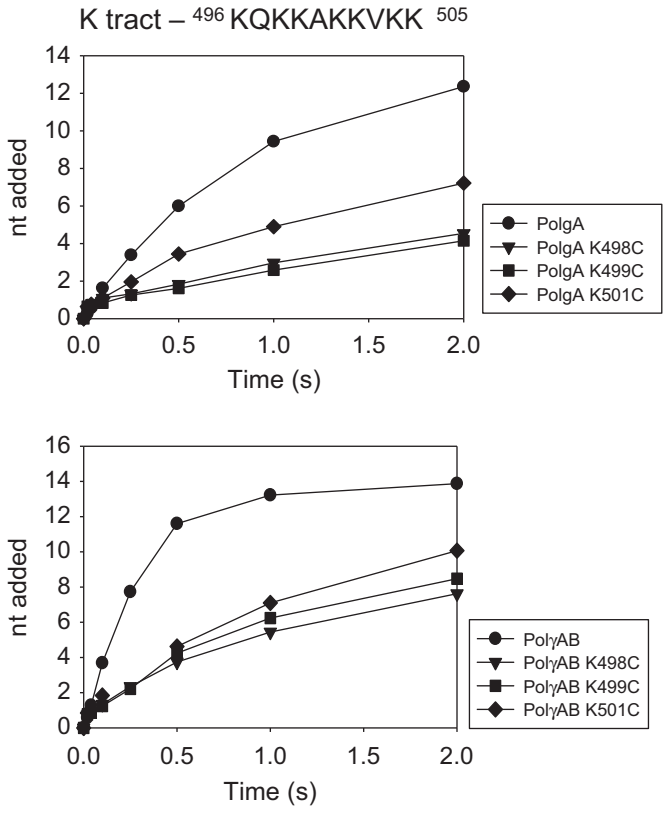

Figure 6. Pre-steady state kinetics assays of K-tract mutants.
Assays were performed on the 65-nt DNA template annealed to a 5′-^{32}P-labeled 25-nt primer and initiated by the addition of dNTPs. DNA synthesis products synthesized by Pol γA variants alone (top panels) or holoenzymes (bottom panels).

The addition of Pol γB partially rescues this defect of the Pol γA mutants and there is relatively less stalling after the addition of one nucleotide, but the mutant proteins remain less processive. Consequently, they synthesize DNA at three- to fivefold slower rates relative to wild-type. The rest of the K-tract mutants show similar activity as the wild-type (Fig 6). Overall, the results indicate that the K-tract is not directly involved in the nucleotide addition catalytic activity, but the inability to interact with upstream DNA decreases the processivity of DNA synthesis. Interestingly, this defect is observed in lysines that are close to mutation Q497H substitution, which is associated with Alpers syndrome (Winterthun *et al*, 2005).

Communication between pol and exo sites

An incorporated NRTI is technically an incorrect nucleotide and should therefore provoke proofreading by Pol γ exonuclease. However, the most toxic nucleotide analog inhibitors, including ddC, are hydrolyzed at significantly slower rates than drugs with lower toxicity, indicating that *exo* contributes to Pol γ-mediated drug toxicity (Feng *et al*, 2001; Lim & Copeland, 2001).

The *exo* domain (residues 170–440) of Pol γ is both spatially separated and structurally distinct from *pol*; the two active sites are 35 Å apart and *exo* consists of an array of antiparallel β-sheets sandwiched between α-helices (Fig 7A). This configuration of *exo* and its distance from *pol* are generally conserved in other members of the DNA Pol I family. When *pol* incorporates an incorrect nucleotide, the 3′-end has to move to *exo* for excision. There must therefore be a mechanism to link recognition of a misincorporation event to shuttling of the 3′-end to *exo*.

Analysis of the Pol γ–DNA structure suggests that an antiparallel hairpin, consisting of residues 835–858, could perform this function. The hairpin is located between *pol* and *exo*, and the hairpin tip contains two adjacent arginines in a conserved hexapeptide ^{851}TRRAVE^{856} (Fig 7; Supplementary Fig S5). In the Pol γ replicating complex, R^{853} reaches into *pol* and forms an H-bond with base pair −1 in the minor groove, as well as with the incoming nucleotide at the +1 position (Fig 7B and C; Supplementary Fig S6). These H-bonds can serve as checkpoints for correct Watson–Crick (W-C) base complementarity. The other conserved arginine, R^{852}, points away from the DNA duplex and is embedded in a deep protein core, forming bipartite H-bonds with residues K^{1107} and S^{1103} in a helix of the fingers subdomain (Fig 7). These interactions may be important in positioning R^{853}. The base of the connecting hairpin is close to the thumb and thus could be able to sense both the thumb rotation and the fingers open–close conformational changes that occur during nucleotide incorporation. These structural features lead us to hypothesize that the antiparallel hairpin may physically and functionally link the base complementarity check with, in the case of misincorporation, shuttling the primer end from *pol* to *exo*. In support of this idea, Pol γA substitutions at R^{852} and R^{853} were found to dramatically reduce polymerase activity and, not surprisingly, are associated with mitochondrial disorders: Patients carrying Pol γA R852C/H display increased mtDNA mutations, and Parkinsonism patients carrying R853W/Q show multiple mtDNA deletions (Davidzon *et al*, 2006; Gonzalez-Vioque *et al*, 2006; Kasiviswanathan *et al*, 2009; Vasta *et al*, 2012). *In silico*, the substitutions R852C/H abrogate the H-bonds that facilitate positioning R853, whereas substitution of R^{853} with the bulkier tryptophan residue abolishes

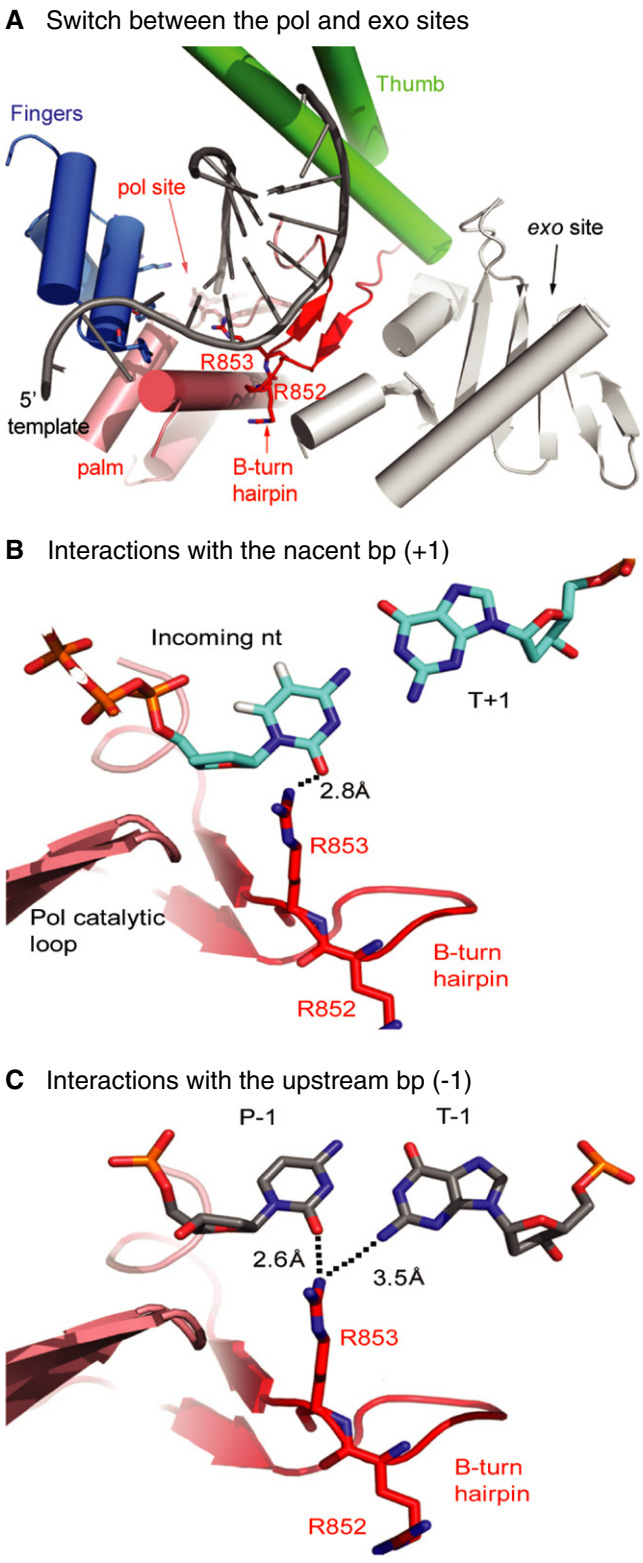

Figure 7. Regulator for *pol* and *exo* activity.

A The β-hairpin is situated between *pol* and *exo* active sties and is connected to the thumb subdomain. R^{852} interacts with residues on the fingers subdomain.

B R^{853} forms H-bonds with the nascent bp of incoming nucleotide and the template residue (T+1).

C Upstream, R^{853} interacts with bp of the T-1 template and P-1 primer residues.

the important H-bond with the −1 base pair. The loss of this checkpoint for base complementarity in *pol* could increase the mutation rate, and/or cause slippage during replication.

The antiparallel hairpin is spatially conserved in other Pol I family members. The Pol γA R^{853} that performs the minor groove checking at base pair −1 is conserved as R^{429} and R^{668} in T7 DNAP and *E. coli* Pol I, respectively (Doublié *et al*, 1998). The amino acid composition of this hairpin is one of the most conserved sequences in known bacterial Pol I family enzymes (TG**R**LSSXXPNLQNIP, the conserved R is bolded), and the sequence of the antiparallel hairpin in Pol γ is highly conserved in mitochondrial polymerases from invertebrates to mammals (Supplementary Fig S5), suggesting a common and important function.

This β-hairpin is seemingly structurally conserved even in polymerases with proofreading activity from other families, such as the Pol B family members bacteriophage RB69 and T4 DNA polymerases (Hogg *et al*, 2007; Subuddhi *et al*, 2008). Studies of the synthesis and editing complexes of RB69 identified a β-hairpin that appears to perform the same function. The β-hairpin of RB69 is located on the surface of the molecule and, although different from Pol γ, may serve as a communicator between the *pol* and *exo* sites (Hogg *et al*, 2007; Subuddhi *et al*, 2008). Additional residues, typically conserved Gln and Asn in Pol I family polymerases, also participate in minor groove readout: Q1102 and N1098 in Pol γ, Q615 and N611 in T7 DNAP, and Q745 and N750 in Taq DNAP. The linearly aligned Arg, Gln, and Asn extend the entire distance of the minor groove of the nascent base pair and are predicted to be critically important to maintain DNA synthesis fidelity.

Allosteric regulatory switch for *pol*/*exo* activities

The conformational changes in the replication complex suggest a structural mechanism for *pol*/*exo* activity regulation by Pol γA–distal Pol γB interface. Mutations on both subunits in this region display severe loss of function in patients. In addition to the Pol γA R232G/H mutant holoenzymes as discussed above, the Pol γB G451E substitution, located in the same interface in the replication complex, shows equivalently decreased synthesis and increased nucleolytic activity defects as the Pol γA R232-containing holoenzyme (Longley *et al*, 2006; Lee *et al*, 2010a; Young *et al*, 2011). Pol γB G451E has a severely reduced association with Pol γA, which decreases the stimulation of catalytic activity and processivity (Longley *et al*, 2006; Young *et al*, 2011). Both G^{451} residues in the Pol γB dimer interact with Pol γA in the replication complex, and therefore, the substitution weakens the holoenzyme: The distal G451E causes a steric clash with E^{230} of Pol γA, whereas the proximal G451E weakens the interaction with the hydrophobic Pol γA L-helix (Fig 8). These studies strongly suggest that the interaction between Pol γA and the distal Pol γB monomer is critical for holoenzyme *pol* activity and that disruption of the subunit interface favors binding of the primer in *exo*. Lack of such interaction in the holoenzyme containing Pol γB G451E substitution makes it structurally resemble the apo enzyme. To investigate this idea, we modeled the transition of Pol γ holoenzyme from the apo to the ternary complex, assuming that the DNA binding to the thumb was unchanged. The resulting complex positions the 3′-end of the primer away from *pol* and 16 Å closer to *exo* (Supplementary Fig S7). This exercise suggests that interactions between Pol γA and distal Pol γB monomer contribute to *pol*/*exo*

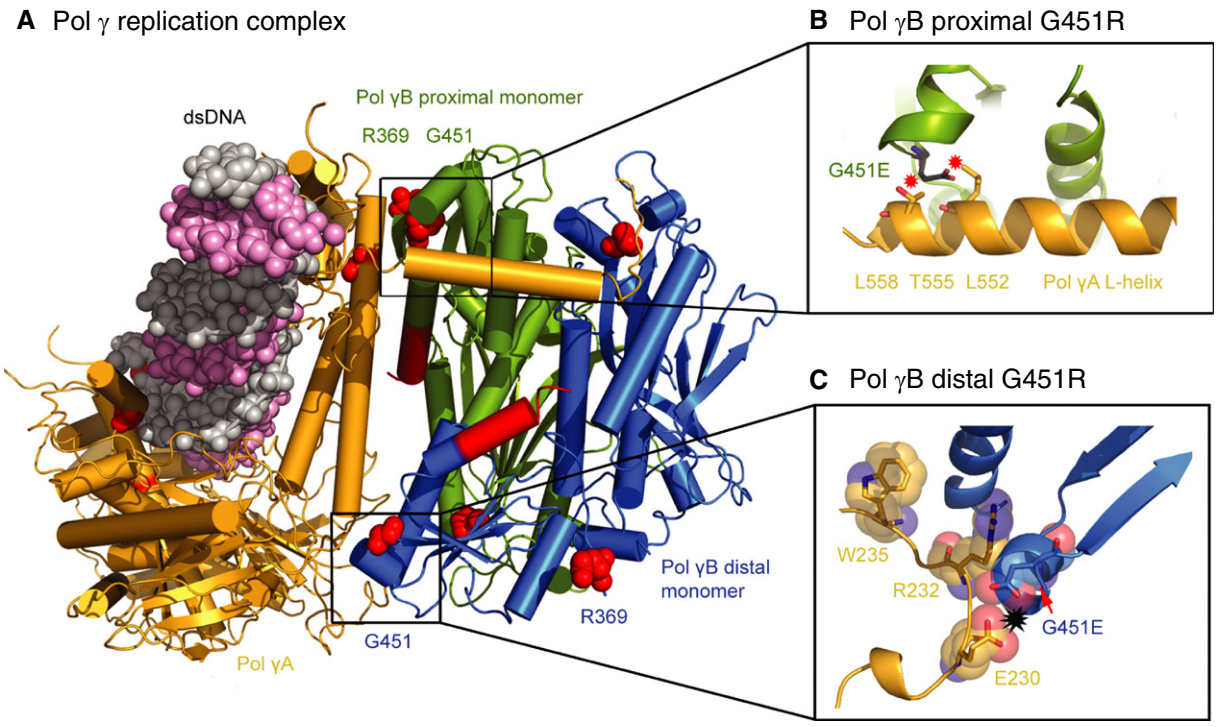

Figure 8. Structural rationalization of deleterious Pol γ mutations implicated in human diseases.

A Pol γB G451E mutations illustrated on the structure of the holoenzyme replication complex.

B The proximal monomer G451E interacts with the L-helix of Pol γA.

C The distal monomer G451E interacts with the Pol γA R^{232} region.

activity regulation. The model thus provides a structural explanation for how Pol γB can simultaneously regulate both *pol* and *exo* activities by serving as an allosteric regulator through dynamic interactions at the Pol γA–distal Pol γB interface.

The ternary structures of Pol γ presented here are the first intact human multi-subunit replicating complexes. The structures reveal that the holoenzyme possesses a strong inter-subunit core that maintains the constant contacts between the catalytic subunit Pol γA and the proximal monomer of Pol γB, which are necessary for highly processive DNA synthesis, but leaves the Pol γA–distal Pol γB monomer interface dynamic, such that the interface can regulate both DNA synthesis and proofreading. Thus, the Pol γA–distal Pol γB monomer interface functions as an allosteric regulator for *pol* and *exo* activities. We show that the nucleoside inhibitor designed against HIV reverse transcriptase binds to Pol γ almost identically as the substrate, providing a structural basis for Pol γ's susceptibility to inhibition by dideoxynucleotides. These structures provide a literal and conceptual framework for assessing the impact of Pol γ mutations implicated in mitochondrial diseases.

Materials and Methods

Cloning and expression

Wild-type and exonuclease-deficient (*exo*$^-$), D198A/E200A Pol γA, lacking residues 1–29 (mitochondrial localization sequence) and 10 of the 13 sequential glutamines (residues 43–52), were placed in pET22b(+) (Novagen). K-tract (^{496}KQKKAKKVKK^{505}) mutants were produced by substituting each lysine to cysteine in *exo*$^-$ Pol γA using the QuikChange kit (Stratagene), resulting in *exo*$^-$ Pol γA K496C, K498C, K499C, K501C, K502C, K504C, and K506C. Clones were transferred into the baculovirus genome using the shuttle vector pBacPak9 (Clontech) The C-terminal His-tagged proteins were synthesized in Sf9 insect cells (Invitrogen), grown at 27°C in SF900-II SFM growth medium, and infected at a density of 1–2 × 10^6 cells/ml. Cells were harvested 72 h post-infection. Selenomethionine-substituted *exo*$^-$ Pol γA was purified by a modification of our earlier protocol (Lee *et al*, 2009). In brief, SF-900 II SFM growth medium (Invitrogen) was exchanged 12 h after infection with unsupplemented Grace's insect medium (Invitrogen), and 50 mg/l L-(+)-Se-Met (Acros) was added. Cells were harvested 48 h after medium exchange. Pol γB-ΔI4 was expressed and purified as described (Lee *et al*, 2009). Selenomethionine-substituted Pol γB-ΔI4 was expressed in *E. coli* B834(DE3) RIL (Novagen) in M9 minimal media supplemented with 100 mg/l L-(+)-Se-Met (Acros).

Protein purification

Pol γA wild-type and variants Pol γA *exo*$^-$, K496C, K498C, K499C, K501C, K502C, K504C and K506C, and Pol γB wild-type and variant ΔI4 were purified by sequential application to TALON (Clontech) for Pol γA *exo*$^-$ and Ni-NTA agarose (Qiagen) for Pol γB-ΔI4, SOURCE S, and Superdex 200 columns (Lee *et al*, 2009). Selenomethionine-substituted *exo*$^-$ Pol γA and Pol γB-ΔI4 were purified similarly. Holoenzyme used for crystallization is formed by combining *exo*$^-$ Pol γA

Table 1. Data collection and refinement statistics.

	Se-Met ddCTP	Native ddCTP	Native dCTP
Wavelength (Å)	0.979 Å	1.0 Å	1.0 Å
Resolution range (Å)	46.14–3.549 (3.676–3.549)	48.68–3.29 (3.48–3.29)	48.48–3.459 (3.718–3.459)
Space group	P 41 21 2	P 41 21 2	P 41 21 2
Unit cell	215.62 215.62 159.148 90 90 90	217.686 217.686 168.49 90 90 90	216.167 216.167 162.72 90 90 90
Total reflections	5,055,152	961,381	1,882,186
Unique reflections	45,635 (4,315)	61,142 (5,694)	53,256 (4,441)
Multiplicity	37.5	3.1	5.8
Completeness (%)	99.60 (96.00)	99.50 (99.96)	99.64 (98.60)
Mean I/sigma(I)	18.09 (3.13)	21.52 (2.07)	18.53 (2.87)
R-merge	0.092	0.067	0.096
R-work	0.2868 (0.3971)	0.2812 (0.3783)	0.2842 (0.4126)
R-free	0.3164 (0.4253)	0.3280 (0.4131)	0.3074 (0.4310)
Number of atoms	14,632	14,632	14,633
Macromolecules			
Proteins	13,622	13,622	13,622
Nucleic acids	983	983	983
Ligand			
Nucleotides triphosphate	27	27	28
Divalent metal ions	2	2	2
Water	0	0	0
Number of residues			
Protein residues	1,741	1,741	1,741
Nucleic acid residues	47	47	47
Nucleotides triphosphate	1 ddCTP	1 ddCTP	1 dCTP
RMS (bonds) (Å)	0.004	0.004	0.003
RMS(angles) (°)	1.13	0.88	0.79
Ramachandran favored (%)	95	99.3	99.0
Ramachandran outliers (%)	4.9	0.69	0.98
Clashscore	18.54	11.75	10.8
Average B-factor	58.30	53.66	61.57
Macromolecules	49.40	46.30	57.60
Nucleic acids	86.90	82.20	99.30

Statistics for the highest resolution shell are shown in parentheses.

and Pol γB-ΔI4 at a 1:2 molar ratio and isolation on Superdex 200. The peak fractions corresponding to 240-kDa complex were pooled and verified by SDS–polyacrylamide gel electrophoresis (SDS–PAGE). Proteins were judged to be ~98% pure. Concentrations of Pol γA and Pol γB were determined spectrophotometrically using extinction coefficients: $\varepsilon_{280} = 2.4379 \times 10^5\ M^{-1}\ cm^{-1}$ and $1.4388 \times 10^5\ M^{-1}\ cm^{-1}$, respectively.

Preparation and crystallization of the Pol γAB–DNA–nucleotide complex

Synthetic DNA oligonucleotides were obtained from Midland Certified (Midland, TX) and IDT (Coralville, Iowa). Nucleic acid scaffolds (Fig 1C) were mixed at equimolar concentrations of template and primer to a final concentration of 1 mM of primer/template DNA and were then annealed by heating to 95°C and slowly cooling to room temperature. ddCTP and dCTP were purchased from TriLink BioTechnologies (San Diego, CA). For crystallization, the *exo*$^-$ Pol γA and Pol γB-ΔI4 complex (40–65 μM) was formed with 1 mM $CaCl_2$, 1 mM ddCTP or dCTP, and 24/28-mer primer/template DNA (60–95 μM) and incubated on ice for ~15 min. Crystals were obtained using the sitting-drop method by mixing the complex at 1:1 volume ratio with a solution: 3% PEG 8000, 150 mM NaCl, 10 mM $CaCl_2$, 100 mM MES pH 6, 2 mM 2-mercaptoethanol, 0.8 M NDSB-201, 1–6% sucrose, and 2% Jeffamine M-600. Crystallization experiments were performed against a

well solution containing 3% PEG 8000, 150 mM NaCl, 10 mM $CaCl_2$, 100 mM MES pH 6, and 2 mM 2-mercaptoethanol at 20°C. Crystals grew to a maximum size of 0.4 × 0.2 × 0.2 mm within 2–4 days. Selenomethionine-substituted *exo*$^-$ PolγABΔI4–DNA-ddCTP was grown similarly except that 2-mercaptoethanol was 50 mM. Before freezing in liquid nitrogen, crystals were cryo-protected by adding a mixture of glycerol and MPD (≤ 20% final) and 1 mM ddCTP/dCTP into the crystallization drop.

Data collection, refinement, and structural determination

X-ray diffraction data were collected at 100 K using synchrotron sources at Advanced Photon Source and Advanced Light Source. Single wavelength anomalous dispersion (SAD) diffraction data were collected at peak of the Se anomalous wavelength (0.979 Å) using the inverse beam method, and the native data were collected at 1.0 Å wavelength. Diffraction data sets were processed with HKL (Minor *et al*, 2006), and data collection statistics are shown in Table 1. The structures were determined using combined phases from molecular replacement and SAD. Forty-two (of 46 total) Se atoms in the holoenzyme were identified, and the combined phases gave a figure of merit 0.704. Phases were further improved by density modification. The final structure was refined using Phenix (Adams *et al*, 2010). The experimental map clearly illustrates density for the double-helical DNA structure (Supplementary Fig S8), and enabled rebuilding of the regions that had undergone structural changes induced by DNA binding. Disordered regions of the holoenzyme are mainly located in the N- or C- terminal and fingers regions. These regions include residues 30–76, 248–261, 317–342, 663–740, 996–1,051, and 1,230–1,239. The disordered regions in Pol γB involve 116 aa in the dimer and again are the same in both structures. They include residues 26–67, 222–228, and 356–361 in chain B and 26–66, 220–226, and 356–367 in chain C.

Kinetic assays

Pre-steady state polymerization assays were carried out using RQF-3 Rapid Chemical Quench Flow instrument (KinTek Co.). Briefly, reactions were initiated by rapid mixing of a pre-incubated Pol γAB–DNA complex (200 nM Pol γA, 800 nM Pol γB) and 50 nM primer/template DNA with 5′-^{32}P-labeled primer with 1 mM dNTP, 10 mM $MgCl_2$ in buffer containing 50 mM Tris acetate pH 7.5, 50 mM potassium glutamate, 0.05% Tween-20, 5% glycerol, and 2 mM DTT. Reactions were incubated at 37°C before being quenched with 0.5 M EDTA. The resulting polymerization patterns were resolved using 24% denaturing PAGE and were visualized by autoradiography. The reactions were carried out with a 65-mer template (CATATTAATTATGATATAGACCCATAATTATATTACTTAGTTGAA TCTCTTCCACTAACCAGCGC) annealed to a 25-mer primer (GCGCTGGTTAGTGGAAGAGATTCAA). Each of the DNA bands up to 17-nt additions was quantified and summed to estimate the number of nucleotides added in each reaction time, and the slopes after one-nucleotide addition are provided as estimates of the DNA synthesis rates.

Accession numbers

'The coordinates of the structures reported here have been deposited in the Protein Data Bank (accession numbers 4ZTU and 4ZTZ).

Supplementary information for this article is available online: http://emboj.embopress.org

Acknowledgements

We thank I Molineux and J Lee and M Morais for critical reading and editing of the manuscript. We thank staff at the beamlines 19-ID and 19-BM at the Advanced Photon Source, Argonne National Laboratory, Argonne, IL, and beamlines 8.8.2 and 8.2.1 at the Advanced Light Source, Lawrence Berkeley National Laboratory, Berkeley, CA. The work is supported by grants from NIH (GM 083703 and GM110591) and Welch Foundation (H-1592) to YWY, and NIH (GM55310) to SSP. MRS was partially supported by the J. B. Kempner Postdoctoral Fellowship.

Author contributions

MRS, VBK, CS, QM, Y-SL, and YWY designed and performed the experiments and analyzed the experimental results. SP and GP performed and analyzed the kinetic data. MRS, SP, and YWY wrote the manuscript.

Conflict of interest

The authors declare that they have no conflict of interest.

References

Adams PD, Afonine PV, Bunkoczi G, Chen VB, Davis IW, Echols N, Headd JJ, Hung LW, Kapral GJ, Grosse-Kunstleve RW, McCoy AJ, Moriarty NW, Oeffner R, Read RJ, Richardson DC, Richardson JS, Terwilliger TC, Zwart PH (2010) PHENIX: a comprehensive Python-based system for macromolecular structure solution. *Acta Crystallogr D Biol Crystallogr* 66: 213 – 221

Astatke M, Grindley ND, Joyce CM (1998) How *E. coli* DNA polymerase I (Klenow fragment) distinguishes between deoxy- and dideoxynucleotides. *J Mol Biol* 278: 147 – 165

Davidzon G, Greene P, Mancuso M, Klos KJ, Ahlskog JE, Hirano M, DiMauro S (2006) Early-onset familial Parkinsonism due to POLG mutations. *Ann Neurol* 59: 859 – 862

Doublié S, Ellenberger T (1998) The mechanism of action of T7 DNA polymerase. *Curr Opin Struct Biol* 8: 704 – 712

Doublié S, Tabor S, Long AM, Richardson CC, Ellenberger T (1998) Crystal structure of a bacteriophage T7 DNA replication complex at 2.2 A resolution. *Nature* 391: 251 – 258

Estep PA, Johnson KA (2011) Effect of the Y955C mutation on mitochondrial DNA polymerase nucleotide incorporation efficiency and fidelity. *Biochemistry* 50: 6376 – 6386

Feng JY, Johnson AA, Johnson KA, Anderson KS (2001) Insights into the molecular mechanism of mitochondrial toxicity by AIDS drugs. *J Biol Chem* 276: 23832 – 23837

Feng JY, Murakami E, Zorca SM, Johnson AA, Johnson KA, Schinazi RF, Furman PA, Anderson KS (2004) Relationship between antiviral activity and host toxicity: comparison of the incorporation efficiencies of 2′,3′-dideoxy-5-fluoro-3′-thiacytidine-triphosphate analogs by human immunodeficiency virus type 1 reverse transcriptase and human mitochondrial DNA polymerase. *Antimicrob Agents Chemother* 48: 1300 – 1306

Ferrari G, Lamantea E, Donati A, Filosto M, Briem E, Carrara F, Parini R, Simonati A, Santer R, Zeviani M (2005) Infantile hepatocerebral syndromes associated with mutations in the mitochondrial DNA polymerase-gammaA. *Brain* 128: 723 – 731

Gellon L, Carson DR, Carson JP, Demple B (2008) Intrinsic 5′-deoxyribose-5-phosphate lyase activity in *Saccharomyces cerevisiae* Trf4 protein with a possible role in base excision DNA repair. *DNA Repair* 7: 187 – 198

Gonzalez-Vioque E, Blazquez A, Fernandez-Moreira D, Bornstein B, Bautista J, Arpa J, Navarro C, Campos Y, Fernandez-Moreno MA, Garesse R, Arenas J, Martin MA (2006) Association of novel POLG mutations and multiple mitochondrial DNA deletions with variable clinical phenotypes in a Spanish population. *Arch Neurol* 63: 107 – 111

Graves SW, Johnson AA, Johnson KA (1998) Expression, purification, and initial kinetic characterization of the large subunit of the human mitochondrial DNA polymerase. *Biochemistry* 37: 6050 – 6058

Graziewicz MA, Longley MJ, Bienstock RJ, Zeviani M, Copeland WC (2004) Structure-function defects of human mitochondrial DNA polymerase in autosomal dominant progressive external ophthalmoplegia. *Nat Struct Mol Biol* 11: 770 – 776

He Q, Shumate CK, White MA, Molineux IJ, Yin YW (2013) Exonuclease of human DNA polymerase gamma disengages its strand displacement function. *Mitochondrion* 13: 592 – 601

Hogg M, Aller P, Konigsberg W, Wallace SS, Doublié S (2007) Structural and biochemical investigation of the role in proofreading of a beta hairpin loop found in the exonuclease domain of a replicative DNA polymerase of the B family. *J Biol Chem* 282: 1432 – 1444

Johnson AA, Tsai Y, Graves SW, Johnson KA (2000) Human mitochondrial DNA polymerase holoenzyme: reconstitution and characterization. *Biochemistry* 39: 1702 – 1708

Johnson AA, Ray AS, Hanes J, Suo Z, Colacino JM, Anderson KS, Johnson KA (2001) Toxicity of antiviral nucleoside analogs and the human mitochondrial DNA polymerase. *J Biol Chem* 276: 40847 – 40857

Kasiviswanathan R, Longley MJ, Chan SS, Copeland WC (2009) Disease mutations in the human mitochondrial DNA polymerase thumb subdomain impart severe defects in mitochondrial DNA replication. *J Biol Chem* 284: 19501 – 19510

Koczor CA, Lewis W (2010) Nucleoside reverse transcriptase inhibitor toxicity and mitochondrial DNA. *Expert Opin Drug Metab Toxicol* 6: 1493 – 1504

Kollberg G, Moslemi AR, Darin N, Nennesmo I, Bjarnadottir I, Uvebrant P, Holme E, Melberg A, Tulinius M, Oldfors A (2006) POLG1 mutations associated with progressive encephalopathy in childhood. *J Neuropathol Exp Neurol* 65: 758 – 768

Lee H, Hanes J, Johnson KA (2003) Toxicity of nucleoside analogues used to treat AIDS and the selectivity of the mitochondrial DNA polymerase. *Biochemistry* 42: 14711 – 14719

Lee HR, Johnson KA (2006) Fidelity of the human mitochondrial DNA polymerase. *J Biol Chem* 281: 36236 – 36240

Lee YS, Kennedy WD, Yin YW (2009) Structural insights into human mitochondrial DNA replication and disease-related polymerase mutations. *Cell* 139: 312 – 324

Lee YS, Johnson KA, Molineux IJ, Yin YW (2010a) A single mutation in human mitochondrial DNA polymerase Pol gammaA affects both polymerization and proofreading activities of only the holoenzyme. *J Biol Chem* 285: 28105 – 28116

Lee YS, Lee S, Demeler B, Molineux IJ, Johnson KA, Yin YW (2010b) Each monomer of the dimeric accessory protein for human mitochondrial DNA polymerase has a distinct role in conferring processivity. *J Biol Chem* 285: 1490 – 1499

Lim SE, Longley MJ, Copeland WC (1999) The mitochondrial p55 accessory subunit of human DNA polymerase gamma enhances DNA binding, promotes processive DNA synthesis, and confers N-ethylmaleimide resistance. *J Biol Chem* 274: 38197 – 38203

Lim SE, Copeland WC (2001) Differential incorporation and removal of antiviral deoxynucleotides by human DNA polymerase gamma. *J Biol Chem* 276: 23616 – 23623

Lim SE, Ponamarev MV, Longley MJ, Copeland WC (2003) Structural determinants in human DNA polymerase gamma account for mitochondrial toxicity from nucleoside analogs. *J Mol Biol* 329: 45 – 57

Longley MJ, Ropp PA, Lim SE, Copeland WC (1998) Characterization of the native and recombinant catalytic subunit of human DNA polymerase gamma: identification of residues critical for exonuclease activity and dideoxynucleotide sensitivity. *Biochemistry* 37: 10529 – 10539

Longley MJ, Nguyen D, Kunkel TA, Copeland WC (2001) The fidelity of human DNA polymerase gamma with and without exonucleolytic proofreading and the p55 accessory subunit. *J Biol Chem* 276: 38555 – 38562

Longley MJ, Clark S, Yu Wai Man C, Hudson G, Durham SE, Taylor RW, Nightingale S, Turnbull DM, Copeland WC, Chinnery PF (2006) Mutant POLG2 disrupts DNA polymerase gamma subunits and causes progressive external ophthalmoplegia. *Am J Hum Genet* 78: 1026 – 1034

McKenzie R, Fried MW, Sallie R, Conjeevaram H, Di Bisceglie AM, Park Y, Savarese B, Kleiner D, Tsokos M, Luciano C, Pruett T, Stotka JL, Straus SE, Hoofnagle JH (1995) Hepatic failure and lactic acidosis due to fialuridine (FIAU), an investigational nucleoside analogue for chronic hepatitis B. *N Engl J Med* 333: 1099 – 1105

Minor W, Cymborowski M, Otwinowski Z, Chruszcz M (2006) HKL-3000: the integration of data reduction and structure solution–from diffraction images to an initial model in minutes. *Acta Crystallogr D Biol Crystallogr* 62: 859 – 866

Murakami E, Feng JY, Lee H, Hanes J, Johnson KA, Anderson KS (2003) Characterization of novel reverse transcriptase and other RNA-associated catalytic activities by human DNA polymerase gamma: importance in mitochondrial DNA replication. *J Biol Chem* 278: 36403 – 36409

Pinz KG, Bogenhagen DF (2006) The influence of the DNA polymerase gamma accessory subunit on base excision repair by the catalytic subunit. *DNA Repair* 5: 121 – 128

Richards FM (1977) Areas, volumes, packing and protein structure. *Annu Rev Biophys Bioeng* 6: 151 – 176

Rouzier C, Chaussenot A, Serre V, Fragaki K, Bannwarth S, Ait-El-Mkadem S, Attarian S, Kaphan E, Cano A, Delmont E, Sacconi S, de Camaret BM, Rio M, Lebre AS, Jardel C, Deschamps R, Richelme C, Pouget J, Chabrol B, Paquis-Flucklinger V (2014) Quantitative multiplex PCR of short fluorescent fragments for the detection of large intragenic POLG rearrangements in a large French cohort. *Eur J Hum Genet* 22: 542 – 550

Steitz TA, Steitz JA (1993) A general two-metal-ion mechanism for catalytic RNA. *Proc Natl Acad Sci USA* 90: 6498 – 6502

Steitz TA (1999) DNA polymerases: structural diversity and common mechanisms. *J Biol Chem* 274: 17395 – 17398

Steitz TA, Yin YW (2004) Accuracy, lesion bypass, strand displacement and translocation by DNA polymerases. *Philos Trans R Soc Lond B Biol Sci* 359: 17 – 23

Stumpf JD, Copeland WC (2013) The exonuclease activity of the yeast mitochondrial DNA polymerase gamma suppresses mitochondrial DNA deletions between short direct repeats in *Saccharomyces cerevisiae*. *Genetics* 194: 519 – 522

Subuddhi U, Hogg M, Reha-Krantz LJ (2008) Use of 2-aminopurine fluorescence to study the role of the beta hairpin in the proofreading pathway catalyzed by the phage T4 and RB69 DNA polymerases. *Biochemistry* 47: 6130 – 6137

Tabor S, Richardson CC (1995) A single residue in DNA polymerases of the Escherichia coli DNA polymerase I family is critical for distinguishing between deoxy- and dideoxyribonucleotides. *Proc Natl Acad Sci USA* 92: 6339 – 6343

Vasta V, Merritt JL, Saneto RP, Hahn SH (2012) Next-generation sequencing for mitochondrial diseases: a wide diagnostic spectrum. *Pediatr Int* 54: 585 – 601

Wang W, Wu EY, Hellinga HW, Beese LS (2012) Structural factors that determine selectivity of a high fidelity DNA polymerase for deoxy-, dideoxy-, and ribonucleotides. *J Biol Chem* 287: 28215 – 28226

Winterthun S, Ferrari G, He L, Taylor RW, Zeviani M, Turnbull DM, Engelsen BA, Moen G, Bindoff LA (2005) Autosomal recessive mitochondrial ataxic syndrome due to mitochondrial polymerase gamma mutations. *Neurology* 64: 1204 – 1208

Young MJ, Longley MJ, Li FY, Kasiviswanathan R, Wong LJ, Copeland WC (2011) Biochemical analysis of human POLG2 variants associated with mitochondrial disease. *Hum Mol Genet* 20: 3052 – 3066

